Solidification of Chill-Cast Al-Zn-Mg Alloys to be Used as Sacrificial Anodes

C. GONZALEZ, O. ALVAREZ, J. GENESCA, and J.A. JUAREZ-ISLAS

In the present research, Al-Zn-Mg alloys were vacuum induction melted and gravity cast into steel molds. Ingots were microstructurally and electrochemically characterized to evaluate their performance as Al-sacrificial anodes for cathodic protection of structures exposed to marine environments. The microstructure observed in as-cast ingots consisted mainly of α-Al dendrites with 0.68 to 2.25 vol pct of τ phase in α-Al matrix and eutectic in interdendritic regions. After heat treatment, the presence of the τ phase increased up to 5 vol pct. Electrochemical efficiencies obtained in Al alloys showed maximum values of 73 and 87 pct in as-cast ingots and heat-treated ingots, respectively. In order to contribute to the development of Al-Zn-Mg anodes, the Al-5.3 at. pct Zn-6.2 at. pct Mg (Al-12 wt pct Zn-5.4 wt pct Mg) alloy was monitored to identify the temperature changes as it cools through phase transformation intervals. Growth temperatures of the phases present in this alloy were employed to predict the structure growing at fixed growth velocity. Predictions of variation of solute concentration with growth velocity in α-Al dendrites were included, too. The results of these analyses help to select alloy composition and to control microstructure in order to develop a new generation of Al-sacrificial anodes free of In and Hg.

I. INTRODUCTION

AL alloys have been widely used for cathodic protection of structures exposed to marine environments against corrosion,[1] and their performance as Al-sacrificial anodes has been directly related to their electrochemical efficiency or anode current capacity.[2] The activity in this field has increased toward the development of new, less costly, and specially pollution-free (without Hg and In) Al anodes with high efficiencies.[3] During the development of the Al anode, several aspects have been considered in order to improve the cathodic-protection properties of Al alloys. For instance, a correlation was observed between macrostructure and electrochemical efficiency. When the macrostructure was of the equiaxed type, the electrochemical efficiency increased and, on the contrary, decreased when the macrostructure was of the columnar type.[4] This behavior was attributed to a more uniform distribution of solute elements in equiaxed grains as compared with solute distribution in columnar grain distribution of solute elements in equiaxed grains, avoiding segregation of elements at grain boundaries. The influence of addition of alloying elements to pure aluminum has also been discussed in terms of improving cathodic-protection properties of Al alloys.[5] For instance, Gurrappa[6] reported that among the commercial Al-alloy anodes, indium-activated Al anodes work satisfactorily in seawater as well as seawater mud, and Mg additions to Al-Zn-In alloys helped to improve their anode efficiency.

It has also been reported[7] that promoting a uniform distribution of fine intermetallic phases in the α-Al matrix on heat-treated Al-Zn-Mg alloys can be a key factor in promoting a good surface activation of the anode avoiding the formation of the continuous, adherent, and protective oxide film on the alloy surface, once in service. The electrochemical efficiency of this alloy showed a value of 82 pct in its heat-treated condition.

On the other hand, Al-Zn-Mg alloys have mainly been studied because of their high-strength properties,[8] and since the first experimental data of the Al-Zn-Mg system by Eger,[9] additional data have been reported considering both phase equilibrium and thermodynamic data.[10] As mentioned previously, Barbucci and co-workers[1,7] introduced the Al-Zn-Mg alloys to be used as Al anodes. They reported that promoting the precipitation of the intermetallic τ in the α-Al solid solution will increase its electrochemical properties. However, details of the solidification history of this type of alloy are scarce in the literature.

In order to contribute to the development of a new generation of Al-sacrificial anodes with high electrochemical efficiencies, a microstructural and electrochemical evaluation of several Al-Zn-Mg alloys is carried out. Then, the alloy with the highest electrochemical efficiency is selected to analyze and to predict conditions for growth of α-Al dendrites, τ phase, and eutectic during chill casting solidification of Al-Zn-Mg alloys. For this purpose, a thermal analysis technique[11] is employed in order to know the temperature changes in the alloy as it cools through phase transformation intervals and to determine the growth temperatures of the phases present in the alloy. The data of this thermal analysis are used to carry out a competitive growth analysis by comparing growth temperatures of dendrites and eutectics at fixed growth velocity for any alloy composition.[12] The structure growing at the higher temperature is determined and the resulting structure predicted for that composition. Then, a predicted variation[13] is presented with growth velocity of solute concentration in the α-Al solid solution.

C. GONZALEZ and J. GENESCA, Professors, are with the Faculty of Chemistry-UNAM, Circuito Escolar S/N, Cd. Universitaria, 04510, Mexico, D.F., Mexico. O. ALVAREZ and J.A. JUAREZ-ISLAS, Professors, are with the Materials Research Institute-UNAM, Circuito Escolar S/N, Cd. Uni-versitaria. Contact e-mail: julioalb@servidor.unam.mmx

Manuscript submitted March 18, 2002.

II. EXPERIMENTAL PROCEDURE

The Al, Zn, and Mg elements of commercial purity (99.5 pct), previously weighed, were placed into a SiC crucible and melted in a resistance furnace under an argon protective atmosphere. The liquid melt was gravity cast into a steel chill mold of dimensions $0.03 \times 0.03 \times 0.10$ m. The selected alloy compositions were chosen in such way that they lie between the maximum concentration of solute at equilibrium (C^{eq}_{max}) and the $\alpha + \tau$ field, as indicated in the phase diagram of Figure 1. The alloy composition of as-cast ingots was determined by atomic absorption spectroscopy analysis, and the results are shown in Table I. During solidification of the alloys, two cromel/alumel type K thermocouples (5×10^{-3} m in diameter), separated 10 mm from tip to tip, were introduced into the liquid melt and the solidification history recorded using an Iotech Tempscan 1100 data acquisition system. The resulting ingots were cut out in sections parallel to the heat flow and the microstructure revealed by electroetching the specimens in a solution containing 10 pct perchloric acid in ethanol (25 V, −10 °C, 20 seconds). The samples were observed under optical (Zeiss-Olympus, D.F., Mexico) and scanning electron (Stereoscan 440, Oxford, England) microscopes. X-ray diffractometry (Siemens 5000, Munich, Germany) was performed on each alloy, using a Cu K_α radiation, an iron filter, and a scan velocity of 0.01 ms^{-1}. The volume percents of phases and eutectics were determined experimentally by using software for image analysis.

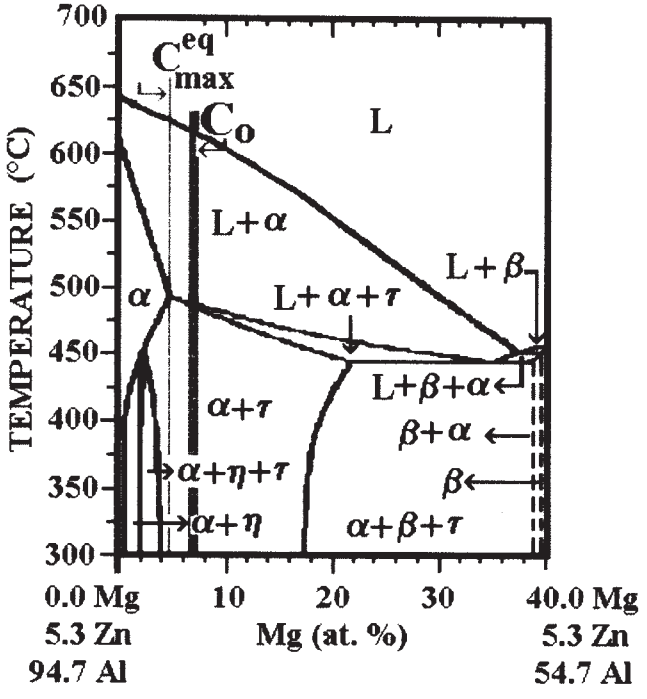

Fig. 1—Vertical sections at 5.3 at. pct of Zn of the Al-Zn-Mg phase diagram, where the position of the alloys under study is indicated.

The electrochemical behavior of Al alloys was investigated in 3 pct NaCl solution simulating seawater at room temperature. Electrochemical impedance spectroscopy measurements were performed using a frequency response analyzer (ACM Instruments, Ltd.) over a frequency range of 10 kHz to 100 mHz (5 points per decade) superimposing a 10 mV AC signal. The equipment was controlled using a PC running electrochemical impedance spectroscopy software. The electrochemical tests were carried out in a three-electrode cell arrangement. The samples of the Al anode (working electrodes) were put in a sample holder presenting an exposed area of 1.227×10^{-4} m^2 to the electrolyte. A platinum gage was used as a counter electrode and a saturated calomel electrode was employed as a reference electrode.

After completion of the full test period, the specimens were cleaned of corrosion products by immersing them for 10 minutes at 80 °C into a solution containing 2×10^{-3} kg of chromium trioxide and 2×10^{-3} l of concentrated phosphoric acid, per liter of water. The specimens were subsequently rinsed in distillated water and then in ethanol, dried, and weighted. The electrochemical efficiency (A-h/kg; A = ampere, h = hour, and kg = kilogram) was calculated according to

$$\text{Electrochemical efficiency} = (C * 1000)/W \qquad [1]$$

where C is the total current charge in ampere-hour and W is the specimen weight loss in kilograms.

III. RESULTS

A. *Microstructure and Electrochemical Efficiency*

The microstructure observed in chill-cast ingots consisted mainly of α-Al dendrites and the eutectic $\alpha + \tau$ in interdendritic regions, as shown in Figure 2. Apart from

Table I. Alloy Compositions and Electrochemical Efficiency of the Alloys under Study

Alloy	Field	Zn (Pct)	Mg (Pct)	Si (Pct)	Cu (Pct)	Al (Pct)	Electrochemical Efficiency	
							As-Cast (Pct)	Heat Treated (Pct)
1	(C^{eq}_{max})	12.0 wt	4.4 wt	0.163 wt	6×10^{-5} wt	bal	68	69
		5.3 at.	5.3 at.	0.168 at.	0.003 at.			
2	$\alpha + \tau$	12.0 wt	5.2 wt	0.198 wt	4×10^{-5} wt	bal	73	87
		5.3 at.	6.2 at.	0.204 at.	0.002 at.			
3	$\alpha + \tau$	12.0 wt	5.4 wt	0.158 wt	1×10^{-4} wt	bal	73	87
		5.3 at.	6.5 at.	0.163 at.	0.005 at.			
4	$\alpha + \tau$	12.0 wt	6.3 wt	0.155 wt	4×10^{-5} wt	bal	78	86
		5.3 at.	7.5 at.	0.160 at.	0.002 at.			

the $\alpha + \tau$ eutectic, the presence of the eutectic α + Si from impurities was detected. These two eutectics were identified by microanalysis. The percent of elements for each eutectic (energy-dispersive X-ray (EDX) microanalysis) and the percent of eutectics (quantitative metallography) in each alloy are shown in Tables II and III, respectively. As can be observed, the amount of eutectics $\alpha + \tau$ (depending of alloy composition) and α + Si (depending of impurities) varied between 11.6 to 15.8 pct and 1.1 to 1.5 pct, respectively.

During solidification of the alloys, the first phase to grow was the α-Al, which developed a dendritic pattern. As the solidification continued, the liquid surrounding the advancing solid/liquid interface was enriched with solute (Zn and

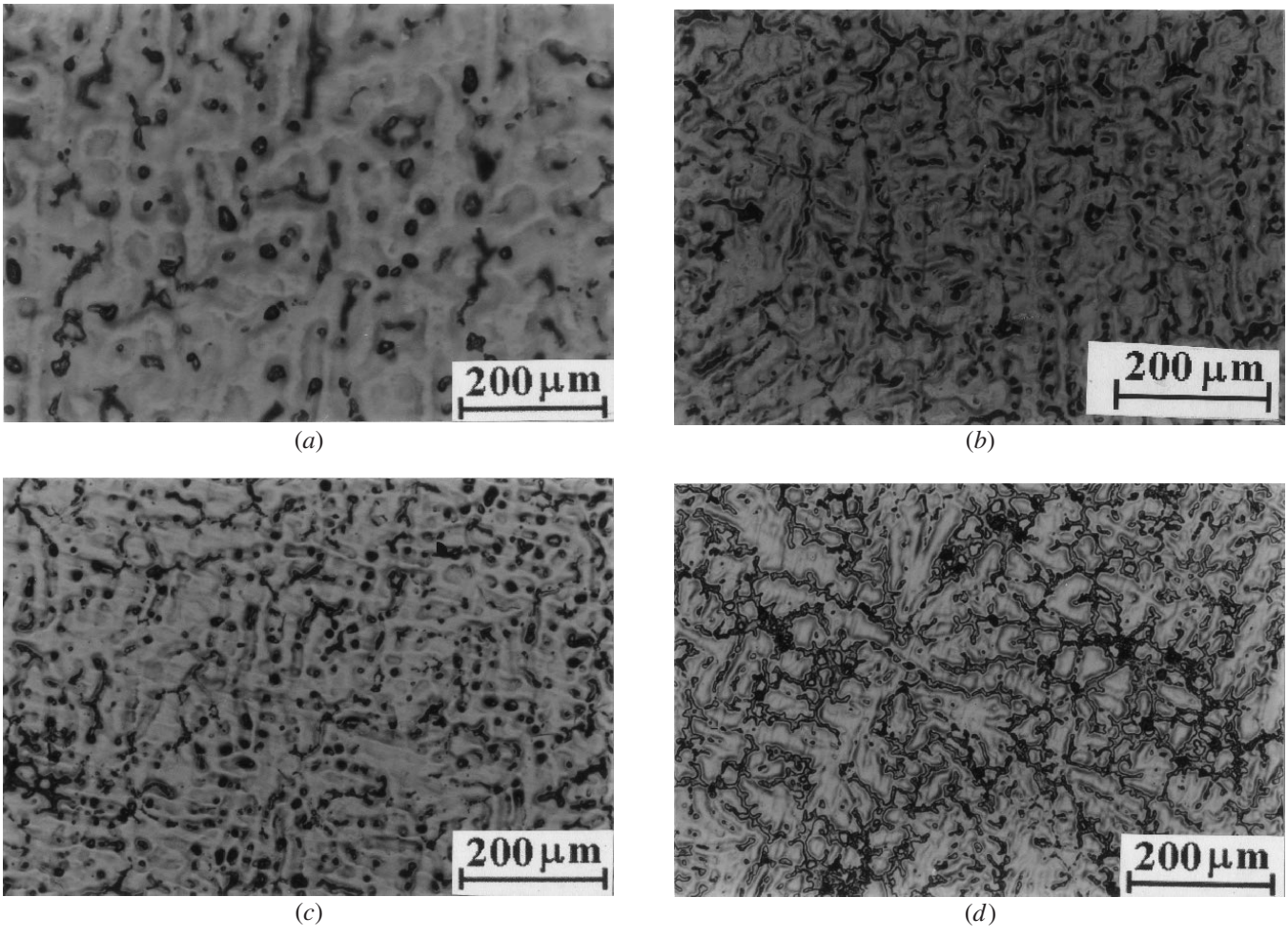

Fig. 2—Microstructure observed in chill-cast ingots of Al-5.3 at. pct Zn with (*a*) 5.3 at. pct Mg, (*b*) 6.2 at. pct Mg, (*c*) 6.5 at. pct Mg, and (*d*) 7.5 at. pct Mg.

Table II. Energy-Dispersive X-Ray Microanalyses of Eutectics (At. pct)

Eutectic	Al	Si	Zn	Mg
$\alpha + \tau$	25.3 ± 0.76	—	37.2 ± 0.45	37.6 ± 0.18
α + Si	84 ± 0.50	16.4 ± 0.61	—	—

Table III. Percentage of Phases of the Alloys under Study

Alloy	α-Al (Pct)	Eutectic (Pct)	Eutectic ($\alpha + \tau$) (Pct)	Eutectic (α + Si) (Pct)	τ Phase	
					As-Cast (Pct)	As-Heat-Treated (Pct)
1	90.8 ± 2.3	10.1 ± 2.1	8.5 ± 0.7	1.5 ± 0.1	0.68	—
2	88.3 ± 3.5	12.3 ± 2.4	10.5 ± 0.6	1.7 ± 0.3	1.17	5.03
3	84.6 ± 2.7	15.2 ± 1.5	13.8 ± 1.1	1.3 ± 0.1	1.74	2.80
4	84.1 ± 3.6	15.8 ± 2.3	14.4 ± 0.2	1.3 ± 0.1	2.25	2.73

Mg plus Si as impurity). As the temperature dropped and a phase transformation temperature was reached, phases such as the eutectic α + Si, the τ phase, and the eutectic $\alpha + \tau$ were formed. The τ phase, which has been reported[7] to be a key factor in promoting a good surface activation of the Al anode, was detected from the X-ray diffractograms, as shown in Figure 3. The percent of τ phase was obtained after integration of the width and height of all the peaks present in the X-ray diffractogram. As can be seen in Table III, the percent of τ phase in as-cast ingots increased as the alloy concentration increased. In heat-treated ingots, the τ phase was not detected in the alloy with a composition $\sim C^{eq}_{\max}$ and reached a maximum value when the percent of Mg was between 6.2 and 6.5 at. pct.

Alloys in both as-cast and as-heat-treated conditions were electrochemically evaluated. The as-cast alloy with a solute concentration close to $C^{eq}_{\max}$ showed an electrochemical efficiency value of 68 pct, while the alloys with compositions $> C^{eq}_{\max}$ reached electrochemical efficiency values up to 78 pct, as shown in Table I. The same table shows electrochemical efficiency values of heat-treated ingots (400 °C, 5 hours). Alloys with a solute concentration close to $C^{eq}_{\max}$ showed the same value of electrochemical efficiency as the as-cast ingot, while alloys with Mg contents between 6.2 and 6.5 at. pct reached a maximum electrochemical efficiency value of 87 pct. This improvement in electrochemical efficiency of the Al alloys under study as compared with the values reported in the literature was attributed to the presence of equiaxed[4,7] structures in as-cast ingots, which allowed a better distribution of solute elements in α-Al matrix, which after heat treatment produced an homogeneous precipitation of fine τ phase in α-Al matrix, which promoted a good surface activation of the anode.

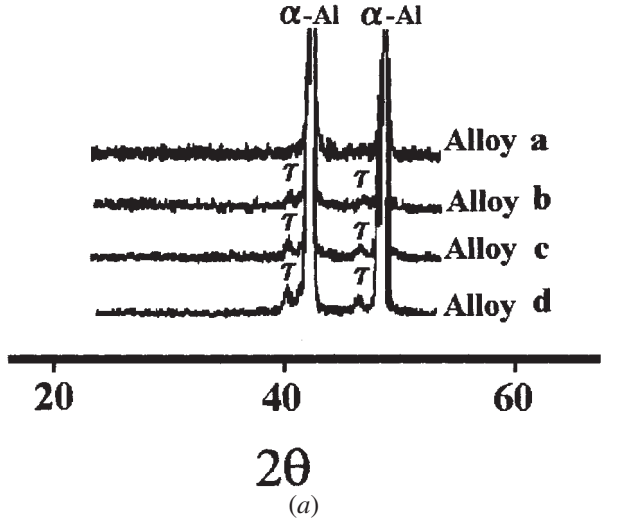

(*a*)

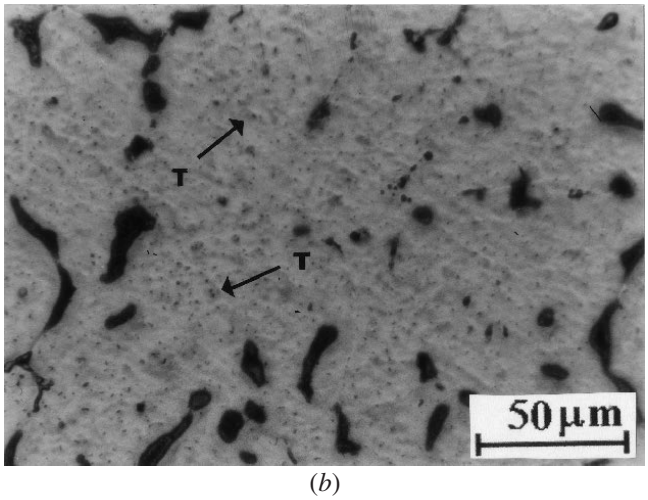

(*b*)

Fig. 3—Results of X-ray diffractometry performed on Al alloys, where the presence of the τ phase is shown.

B. *Solidification*

In order to contribute to the development of Al alloys to be used as Al-sacrificial anodes, the Al-5.3 at. pct Zn-6.2 at. pct Mg alloy, which showed the highest efficiency and the lowest amount of solute, was chosen to monitor its solidification path.

From the outcome of the thermocouples inserted in the liquid melt during solidification of the alloy, a plot of temperature *vs* time was obtained, as shown in Figure 4(a). The thermal arrest indicated by the change in slope of region A resulting from the passage of the solidification front, indicated the growth temperature of the α phase, $T_{G,\alpha}$, giving a value of 612.5 °C. The thermal arrest indicated by the change in slope of region D was taken as the growth temperature, for the ($\alpha + \tau$) eutectic, $T_{G,Eu1}$, giving a value of 443.5 °C. These two changes in slopes identified the two main phases present in the as-cast ingots. Two other changes in slopes were observed in regions B and C, giving temperatures of 575.8 °C and 487.0 °C, representing the growth temperatures for the eutectic α + Si, $T_{G,Eu2}$, and τ phase, $T_{G,\tau}$, respectively. The cooling rate curve shown in Figure 4(b) indicates the beginning of solidification (peak A), and the other peaks B, C, and D represent the range over which a phase formation takes place and the end of solidification, which was completed in approximately 125 seconds.

From the vertical section at 5.3 at. pct of Zn of the Al-Zn-Mg phase diagram (Figure 1[14]), with 6.2 at. pct Mg, it was confirmed that the thermal arrest temperatures of 612.5 °C and 443.5 °C corresponded to the dendrite and eutectic growth temperatures, respectively, whereas the temperature of 487.0 °C indicated the growth temperature of the τ phase, similar to the temperature of 489 °C reported by Droenen and Ryum.[15]

C. *Competitive Growth*

The growth temperatures obtained from the cooling curve of Figure 4 were employed to predict the growth temperature limits of the α-Al, τ phase, and eutectics. For this purpose, a competitive growth analysis was employed.[16] By comparing growth temperatures of dendrites, τ phase, and eutectics at fixed growth velocity for any alloy composition, the structure growing at the higher temperature was determined and the resulting structure predicted for that composition.

The eutectic growth temperature, $T_{G,Eu}$, was predicted[17] and found experimentally[18] to conform with

$$T_{Eu} - T_{G,Eu} = C_1 V^{1/2} \qquad [2]$$

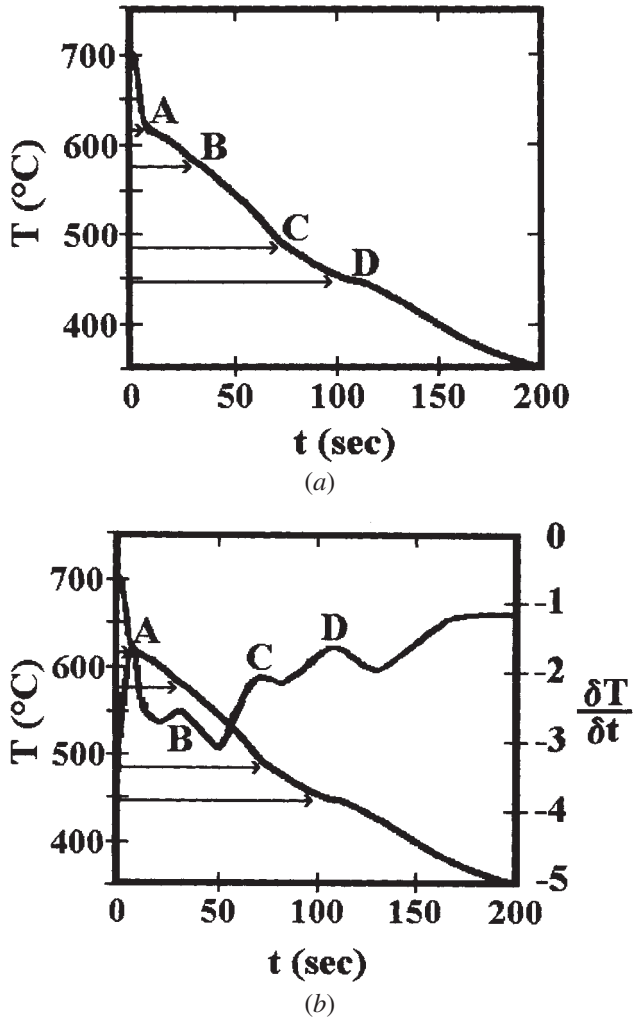

Fig. 4—(*a*) Plot of temperature *vs* time for an Al-5.3 at. pct Zn-6.2 at. pct M. A, B, C, and D represent the thermal arrest temperatures for the α phase, the eutectic α + Si, the τ phase, and the eutectic $\alpha + \tau$, respectively. (*b*) Cooling rate curve.

where T_{Eu} is the equilibrium eutectic temperature, V is the growth velocity, and C_1 is a constant for a given system. The constant C_1 for the Eu_1 and Eu_2 showed a value of 0.0964 $Ks^{1/2}$ $\mu m^{-1/2}$ and 0.1205 $Ks^{1/2}$ $\mu m^{-1/2}$, respectively, for a solidification front velocity of 154 μms^{-1} and $T_{EU} - T_{G,Eu} = 1.2$ and 1.5 K, for the Eu_1 and Eu_2, respectively. These values of 0.0964 and 0.1205 $Ks^{1/2}$ $\mu m^{-1/2}$ are between those values ranging from 0.023 to 0.128 $Ks^{1/2}$ $\mu m^{-1/2}$ measured for the Al-Al_2Cu and Al-Zn eutectics.[19,20]

The corresponding relationship for a dendrite or intermetallic growth is more complex but can be represented by

$$T_{L,\alpha} - T_{G,\alpha} = DG/V + C_2 V^n \qquad [3]$$

where T_L is the alloy liquidus temperature for the growing dendrites or intermetallics, D is the liquidus diffusion coefficient, taken as 3.0×10^{-9} m^2s^{-1},[21] G is the temperature gradient (5×10^{-2} Km, from the experiments), V is the solidification front velocity, C_2 is a constant for a given alloy composition, and n depends on growth morphology and regime but is typically close to 0.5. The constant K_2 for the

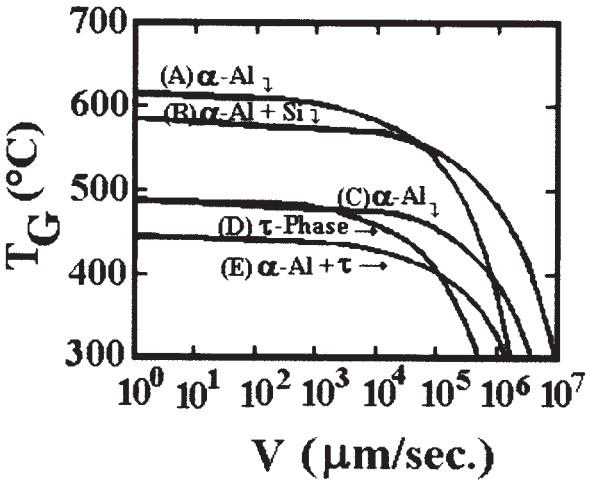

Fig. 5—Growth temperature as a function of growth velocity in Al-5.3 at. pct Zn-6.2 at. pct Mg ($G = 5 \times 10^{-2}$ Km^{-1}) for α-Al solid solution, τ phase, and eutectics α + Si and $\alpha + \tau$.

α-Al and τ phase showed a value of 0.241 and 0.1004 $Ks^{1/2}$ $\mu m^{-1/2}$, respectively, for a solidification front velocity of 154 μm/s and $T_{L,\alpha} - T_{G,\alpha} = 3.0$ and 1.25 K, for the α-Al and τ phase, respectively.

The limiting condition for single-phase growth at the same temperature as a eutectic is obtained by solving Eq.[2] and [3] simultaneously to give the limiting growth velocity as the solution of

$$T_{L,\alpha} - T_{G,Eu} = DG/V + C_2 V^n - C_1 V^{1/2} \qquad [4]$$

Figure 5 shows the result of this competitive growth analysis in terms of the growing temperature for the α-Al, the eutectic α + Si, the τ phase, and the eutectic $\alpha + \tau$ as a function of solidification front velocity. Table IV shows constant values C_1 and C_2 for the alloy under study with $V = 154.7$ μms^{-1}.

Curves A and B represent the competitive growth analysis between the α-Al dendrites and the eutectic α + Si, which was formed from impurities. As can be seen, the α-Al phase grew as the predominant phase throughout the solidification front velocities kept during the experiments. These α-Al dendrites grew freely in the liquidus $+\alpha$ region. Curves C and D represent the competitive growth analysis of the α phase and the τ phase just when solidification of the alloy reached the region L + α + τ, indicating that both the α phase and the τ phase grew simultaneously to solidification from velocities close to 1000 μms^{-1}. Curve E shows the growth temperature as a function of solidification front velocity for the eutectic $\alpha + \tau$, in which it is predicted that this phase will be the dominant phase only at very high solidification front velocities.

The results of this analysis suggest that by a proper selection of alloy composition, which must be higher than C^{eq}_{max}, and by keeping solidification front velocities where the α phase and the τ phase growth simultaneously, the resulting structure will consist mainly of α-Al dendrites with some τ phase in the α-Al matrix, with the advantage of being able to manipulate, with further heat treatments, the amount of

Table IV. Constants C_1 and C_2 for the Alloy under Study (V = 154.7 μm/s)

Specie	$T_{Eu} - T_{G,Eu}$ (K)	C_1 (Ksec$^{1/2}$/ μm$^{1/2}$)	$T_{L,\alpha} - T_{G,\alpha}$ (K)	C_2 (Ks$^{1/2}$/μm$^{1/2}$)
α dendrite	—	—	3.00	0.2410
τ phase	—	—	1.25	0.1004
α + Si	1.20	0.0964	—	—
$\alpha + \tau$	1.50	0.1205	—	—

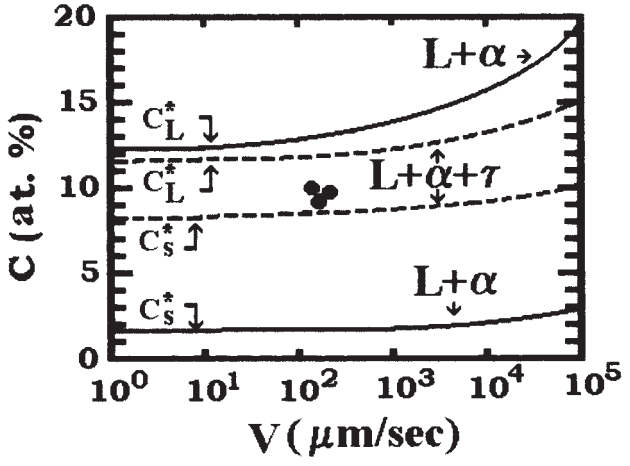

Fig. 6—Predictions of C_s^* as a function of growth velocity for the Al-5.3 at. pct Zn-6.2 at. pct Mg, for regions L + α and L + α + τ of the vertical sections at 5.3 at. pct of Zn of the Al-Zn-Mg phase diagram.

precipitates present in the α-Al matrix. These precipitates will play the role of breaking and avoiding the formation of the continuous, adherent, and protective oxide film on the Al anode, once in service.

D. *Prediction of Solute Concentration*

Kurz *et al.*[13] modeled the problem of constrained dendrite growth at velocities up to the absolute stability limit. The tip concentration in the melt is given by

$$C_L^* = C_o/[1 - p\mathrm{Iv(P)}] \quad [5]$$

and

$$C_s^*(= kC_L^*) \quad [6]$$

where Iv(P) is the Ivantsov function, P (= $VR/2D$) is the solute Peclet number, and p (= $1 - k$), is the complementary partition coefficient. The unknowns P and R are given by the solution of

$$V^2 K_1 + VK_2 + G = 0 \quad [7]$$

where $K_1 = \pi\Gamma/P^2D^2$, $K_2 = mC_o p\xi_c/D[1 - p\mathrm{Iv(P)}]$ with $\xi_c = 1 - 2k/\{[1 + (2\pi/\mathrm{P})]^{1/2} - 1 + 2k\}$, and G is the temperature gradient. Equation [7] was solved numerically by employing material constraint values of $\Gamma = 1.06 \times 10^{-7}$ Km,[9] $D = 3 \times 10^{-9}$ m^{2}s^{-1},[21] m and k were taken as m = -5.55 K at. pct^{-1} and $k = 0.143$ for the region L + α and $m = -3.0$ K at. pct^{-1}, and $k = 0.687$ for the region L + α + τ[14] and from the experiments $G = 5 \times 10^{-2}$ Km^{-1} and C_o = 11.5 at. pct.

The result of this analysis is shown as a plot of alloy concentration as a function of solidification front velocity, in Figure 6, where predictions for C_s^* are given for both regions L + α and L + α + τ. Predictions C_s^* for the region L + α showed that the maximum concentration of Zn + Mg retained in solid solution was close to 2 at. pct, for a solidification front velocity of ~150 μms^{-1}. On the other hand, predictions of C_s^* for the region L + α + τ showed that the maximum concentration of Zn + Mg retained in solid solution was close to 8.2 at. pct, for a solidification front velocity of ~150 μms^{-1}. As can be observed, predictions of C_s^* for region L + α + τ are closer to the experimental results (solid circles) of Zn + Mg retained in solid solution, as determined by wavelength dispersive X-ray microanalysis.

IV. DISCUSSION

The thermal analysis[22] performed on Al-Zn-Mg alloys can be employed to monitor important events during solidification of an alloy, detecting a part from the expected phase transformations (*i.e.*, α-Al, τ phase, and eutectic $\alpha + \tau$ in this work) and unexpected phases formed from impurities. In addition to this information, accurate data of growth temperature for each phase is obtained, which can be employed, together with experimental data, to predict growth temperature limits of phases by means of a competitive growth analysis. This growth temperature and its dependence on growth velocity are key parameters in determining which of various alternative solidification structures is selected by the competitive growth analysis.[23] In the Al-5.3 at. pct Zn-6.2 to 6.7 at. pct Mg alloys, it was detected that solidification front velocities between 10^2 and 10^3 μms^{-1} will be enough to produce a simultaneous growth of the α-Al and the τ phase, when the solidification of the alloy reached the L + α + τ region. The α-Al solid solution and precipitates of τ phase are the main structures to be considered in the design of new Al-Zn-Mg alloys for cathodic protection applications.

Another useful tool to be considered during the design of this alloy is the prediction of tip concentration as a function of solidification front velocity.[10] For instance, in the alloys under study, predictions of Zn + Mg for the region L + α + τ were close to those determined experimentally; the slightly lower values of predictions reflected the fact that the model did not take into account back-diffusion of solute in the solidified solid.[24] The knowledge of the amount of solute in solid solution can be used to find a relationship between matrix solute content and the maximum fraction of precipitates that form during aging. For this aim, Bjorneklett *et al.*,[21] proposed a relationship for the maximum fraction of precipitates that form during aging, of the type $\Delta f_p = k_1[C_m \cdot C^0{}_m]^3$. For our experimental conditions, the constant k_1 achieved a value of 0.1399 vol pct at. pct^{-1}.

V. CONCLUSIONS

1. As-cast Al-Zn-Mg alloys showed a microstructure that consisted of α-Al dendrites and eutectic $\alpha + \tau$ in interdendritic regions with a low fraction of α + Si, from impurities. This alloy showed an outstanding electrochemical behavior, reaching values of electrochemical efficiency up to 73 pct.
2. The thermal analysis performed in the alloys under study indicated temperature changes in the alloy as it cools through phase transformation intervals, giving growth temperatures for the α phase, the eutectic α + Si, the τ phase, and the eutectic $\alpha + \tau$ of 612.5 °C, 575.8 °C, 487.0 °C, and 443.5 °C, respectively.
3. The competitive growth analysis performed in an Al-5.3 at. pct Zn-6.2 at. pct Mg alloy showed that when solidification of liquid melt reached the L + $\alpha + \tau$ region, both phases α and τ grew simultaneously up to solidification front velocities close to 1000 μm/s.
4. Predictions for C_s^* (Zn + Mg) as a function of solidification front velocity, carried out in region L + $\alpha + \tau$, showed values similar to predictions, reflecting the fact that the model did not take into account back-diffusion. Prediction of solute concentration can conceivably be used to predict concentration of precipitates during aging.
5. As-heat-treated Al-5.3 at. pct Zn-6.2 at. pct Mg alloy with a volume fraction of τ phase in the α-Al solid solution of 5.03 showed an electrochemical efficiency of 87 pct.

ACKNOWLEDGMENTS

The authors acknowledge the financial support from the Dirección General de Apoyo al Personal Académico (DGAPA) through Grant No. IN102601 and Consejo Nacional de Ciencia y Tecnología (CONACYT) through Grant No. NC-204. We also thank Mr. Caballero and Eng. L. Baños for carrying out the photographic and X-ray work, respectively.

NOMENCLATURE

C	total current charge (amp-h)
C_1, C_2,	constants for a given system ($Ks^{1/2}\ m^{-1/2}$)
C^{eq}_{max}	the maximum concentration of solute at equilibrium
C_L^*	liquidus tip concentration (wt pct or at. pct)
C_0	concentration (wt pct or at. pct)
C_s^*	solidus tip concentration (wt pct or at. pct)
D	diffusion coefficient in the liquid (m^2s^{-1})
G	temperature gradient (Km)
Iv(P)	is the Ivantsov function
k	partition coefficient
k_1	constant
K_1	a constant ($= \pi/P^2D^2$)
K_2	a constant ($= mC_o p\xi_c/D[1 - p\mathrm{Iv}(P)]$)
m	liquidus slope (°C/wt pct or °C/at. pct)
n	a constant that depends on growth morphology and regime
p	complementary partition coefficient.
P	solute Peclet number
T_G	growth temperature of dendrites, intermetallic or eutectics (°C or K)
T	equilibrium liquidus, intermetallic or eutectic temperature (°C or K)
V	solidification front velocity (ms^{-1})
W	specimen weight loss (kg)
ξ_c	a constant ($= 1 - 2k/\{[1 + (2\pi/P)^2]^{1/2}\}$)
Γ	Gibbs–Thompson coefficient (Km)
Δf_p	fraction of precipitates that form during aging
C_m	mean solute concentration in the matrix (wt pct or at. pct)
C_m^0	matrix solute content in stabilized base material (wt pct or at. pct)

REFERENCES

1. G. Bruzzone, A. Barbucci, and G. Cerisola: *J. Alloys Compounds*, 1997, vol. 247, pp. 210-16.
2. S. Valdes, J. Genesca, B. Mena, and J.A. Juarez-Islas: *J. Mater. Eng. Performance*, 2000, vol. 10 (5), pp. 596-601.
3. K. Ravidran and A.G. Gopalakrishna: *Fishery Technol*., 1987, vol. 24, pp. 1-4.
4. D.R. Salinas, S.G. Garcia, and J.B. Bessone: *J. Appl. Electrochem*., 1999, vol. 29 (9), pp. 1063-71.
5. D.R. Salinas and J.B. Bessone: *Corrosion*, 1991, vol. 47 (9), pp. 665-74.
6. I. Gurrappa: *Corr. Prevention Control*, 1997, June, pp. 69-80.
7. A. Barbucci, G. Cerisola, G. Bruzzone, and A. Saccone: *Electrochemica Acta*, 1997, vol. 42 (15), pp. 2369-80.
8. H. Liang, S.-L. Chen, and Y.A. Chang: *Metall. Mater. Trans. A*, 1997, vol. 28A, pp. 1725-34.
9. G. Eger: *Int. Z. Metallogr*., 1993, vol. 4, pp. 50-128.
10. D.A. Petrov: in *Ternary Alloys*, G. Petzow and G. Effenberg, eds., ASM INTERNATIONAL, Materials Park, OH, 1993, vol. 7, pp. 57-71.
11. C. Labrecque and M. Gagné: *AFS Trans*., 1998, vol. 106, pp. 83-90.
12. J.A. Juarez-Islas and H. Jones: *Inst. Met*., 1988, vol. 421, pp. 492-95.
13. W. Kurz, B. Giovanola, and R. Trivedi: *Acta Metall*., 1986, vol. 34 (5), pp. 823-30.
14. G.M. Kuznetsov, A.D. Barsukov, G.B. Krivosheeva, and E.G. Dieva: *Izv. Akad. Nauk, SSSR Metall*., 1986, vol. 4, pp. 198-200.
15. P.E. Droeneb and N. Ryum: *Metall. Mater. Trans. A*, 1994, vol. 25A, pp. 521-30.
16. J.A. Juarez-Islas: *J. Mater. Sci*., 1994, vol. 26, pp. 5004-09.
17. K.A. Jackson and D. Hunt: *TMS-AIME*, (1966), vol. 236, p. 1129.
18. W. Kurz and D.J. Fisher: *Int. Mater. Rev*., 1979, vol. 24, p. 177.
19. A. Moore and R. Elliot: *The Solidification of Metals*, The Iron and Steel Institute, London, 1968, p. 167.
20. M. Tasa and J.D. Hunt: *J. Cryst. Growth*, 1976, vol. 34, p. 38.
21. B.J. Bjorneklett, O. Grong, O.R. Myhr, and A.O. Klñuken: *Metall. Mater. Trans. A*, 1999, vol. 30A, pp. 2667-77.
22. A.M. Samuel, P. Ouellet, F.H. Samuel, and H.W. Doty: *AFS Trans*., 1977, vol. 156, pp. 951-62.
23. A. Juarez-Hernandez and H. Jones: *Metall. Mater. Trans. A*, 2000, vol. 31A, pp. 327-28.
24. H.D. Brody and M.C. Flemings: *Metall. Trans. A*, 1981, vol. 12A, p. 965.